DOI: 10.1002/ejic.200900614

$BiVO_4$ Hollow Nanospheres: Anchoring Synthesis, Growth Mechanism, and Their Application in Photocatalysis

Wenzong Yin,[a] Wenzhong Wang,*[a] Meng Shang,[a] Lin Zhou,[a] Songmei Sun,[a] and Lu Wang[a]

Keywords: Bismuth / Vanadates / Nanostructures / Template synthesis / Photochemistry

An anchoring method was developed to synthesize monoclinic $BiVO_4$ (*m*-$BiVO_4$) hollow spheres with a size of about 700 nm by employing colloidal carbon spheres (CCSs) as hard templates. The influence of synthesis conditions and the growth mechanism were investigated with XRD, TEM, and SEM through a series of comparison experiments. It was found that two-stage heat treatment was essential for the synthesis of $BiVO_4$ hollow nanospheres. The Bi^{3+} ions were firstly adsorbed on the surface of the CCSs and worked as anchors in the first stage (80 °C). In the second stage (100 °C), the VO_3^- ions reacted with the anchored Bi^{3+} ions, and amorphous $BiVO_4$ nanoparticles were thus precipitated on the CCSs surface. The analysis on the calcination process revealed that calcination promoted the crystallization of amorphous $BiVO_4$ into *m*-$BiVO_4$ crystals at 236 °C and removed the CCSs at 353 °C. The as-prepared $BiVO_4$ hollow nanospheres exhibited higher photocatalytic activity than $BiVO_4$ prepared by the aqueous method and by a solid-state reaction in the degradation of rhodamine B and acetaldehyde, which could be attributed to their higher BET surface area (5.85 $m^2 g^{-1}$) and larger band gap (2.36 eV). Given the general adsorption of metal ions on the CCSs surface, this anchoring method could be extended to synthesize other hollow-structured multicomponent oxides.

Introduction

Hollow micro-/nanostructures have found diverse applications in rechargeable batteries,[1] sensors,[2] catalysis,[3] drug delivery,[4] and biomedical imaging[5] because of their special characteristics that include low density, high surface area, distinct optical properties, and low coefficients of thermal expansion, and refractive index.[6] These promising applications have in turn catalyzed the exploration of both new synthetic approaches and new hollow structures. The ever-reported synthetic approaches can be divided into four categories:[6b] (1) conventional hard template synthesis, (2) sacrificial template synthesis, (3) soft template synthesis, and (4) template-free methods. Though there are many new methods, the conventional hard template method is still prevalent due to the straightforward and facile procedures. Among the commonly employed hard templates, colloidal carbon spheres (CCSs) are popular because the negatively charged –OH and –C=O groups on their surface exhibit intense adsorption of metal ions and thus free the CCSs from further surface modification.

Since the first preparation of CCSs by Sun et al.,[7] CCSs have been widely applied as hard templates in the fabrication of hollow spheres. However, most of them are simple metal oxides[8] that can be easily achieved merely by calcining the CCSs with adsorbed metal ions on their surface. Multicomponent oxide hollow spheres have rarely been synthesized with this method to date because of complex synthesis procedures and indistinct growth mechanism. Li et al.[9] prepared ferrite hollow spheres MFe_2O_4 (M = Ni, Co, Mn, Zn) by direct adsorption of Fe^{3+} and M^{2+} on the surface of CCSs followed by a calcination process to remove the CCSs and transformed the metal ions into pure ferrites. Shang et al.[10] synthesized cage-like Bi_2WO_6 hollow nanospheres through one-step precipitation of Bi_2WO_6 on the surface of CCSs at 160 °C and subsequent calcination at 450 °C. Both of these syntheses involved one-step precipitation of either metal ions or final product on the surface of the CCSs. However, such a one-step precipitation method fails to yield CCSs with surfaces coated with $BiVO_4$, let alone to synthesize $BiVO_4$ hollow spheres. CCSs generally exhibit significant adsorption of metal cations.[8b,8c] Therefore, multicomponent oxides can be precipitated on the surface of the CCSs through a two-step process: (1) precipitation of metal ions on the surface of the CCSs through electrostatic attraction to work as anchors and (2) introduction of anions that contain other target elements to react gradually with the anchored metal ions and thus settle the terminal product or its precursor on the sur-

[a] State Key Laboratory of High Performance Ceramics and Superfine Microstructure, Shanghai Institute of Ceramics, Chinese Academy of Sciences,
1295 Dingxi Road, Shanghai 200050, P. R. China
Fax: +86-21-5241-3122
E-mail: wzwang@mail.sic.ac.cn
Supporting information for this article is available on the WWW under http://dx.doi.org/10.1002/ejic.200900614.

face of the CCSs. Subsequently, hollow spheres could be achieved after removing the CCSs by calcination.

According to the above proposition, here we use the synthesis of $BiVO_4$ hollow nanospheres as an example to illustrate the anchoring method. The growth mechanism was revealed in detail, which demonstrated the necessity of the two-step precipitation process for the preparation of $BiVO_4$ hollow nanospheres. The as-prepared $BiVO_4$ hollow nanospheres exhibited high photocatalytic efficiency not only in the degradation of rhodamine B (RhB) but also in the decomposition of acetaldehyde (CH_3CHO) under visible-light irradiation.

Results and Discussion

Characterization of the CCSs and the $BiVO_4$ Hollow Nanospheres

The TEM image of the CCSs is shown in Figure S1. The CCSs display regular spherical shapes. The diameter of these CCSs is about 600 nm. Zeta potential analysis on the CCSs indicates that the surface of the CCSs are negatively charged at room temperature in EG (ethylene glycol) (pH = 7, ζ = –32.0 mV).

Figure 1a,c represent the XRD patterns of the $BiVO_4$-precipitated CCSs before and after calcination, respectively. The obvious bump between 25 and 35° (Figure 1a) indicates that the $BiVO_4$ on the surface of the CCSs is amorphous before calcination. The XRD pattern of the product calcined at 350 °C for 2 h shows diffraction peaks with a sharp shape and high intensity (Figure 1c). All the diffraction peaks in Figure 1c can be indexed to monoclinic $BiVO_4$ (*m*-$BiVO_4$, JCPDS cards no. 14–0688), suggesting the successful preparation of *m*-$BiVO_4$ crystals. Further, the two XRD patterns imply the leading role of calcination in the crystallization of amorphous $BiVO_4$ into *m*-$BiVO_4$.

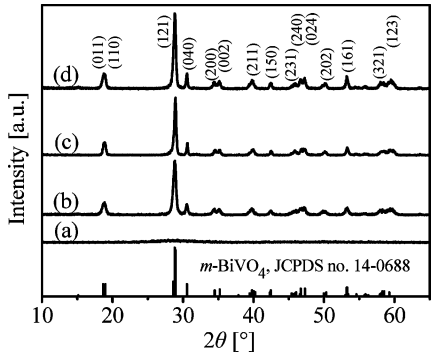

Figure 1. XRD patterns of the as-prepared $BiVO_4$-precipitated CCSs (a) without calcination and with 2 h of calcination at 236 °C (b), at 350 °C (c), and at 450 °C (d).

Figure 2 shows the morphology and microstructure of the as-prepared *m*-$BiVO_4$ crystals. The panoramic TEM image in Figure 2a reveals the hollow structures of the spherical *m*-$BiVO_4$ crystals. The magnified image (inset of Figure 2a) shows that these hollow spheres possess an outside diameter of about 700 nm and a shell thickness of 100–150 nm. It is clear that the inside diameter is 100–200 nm, which is smaller than the diameter of the original CCS templates, which might be attributed to the densification of the amorphous $BiVO_4$ in the shell during the calcinations.[8a] In addition, some of the $BiVO_4$ hollow nanospheres are broken, which enables the observation of hollow structures by SEM images. Figure 2b represents the SEM images of the as-prepared $BiVO_4$ hollow nanospheres. The hollow structures were clearly confirmed by the broken nanospheres. The magnified image (inset of Figure 2b) shows that the shell consists of spherical nanoparticles with a size of about 100–150 nm and only one layer of spherical particles packs along the radius in the shell. This is just in agreement with the thickness of the shell observed in the TEM images. To confirm the microstructure of the shell, selected-area electron diffraction (SAED) was carried out on the hollow nanosphere shown in Figure 2c. The SAED pattern (top

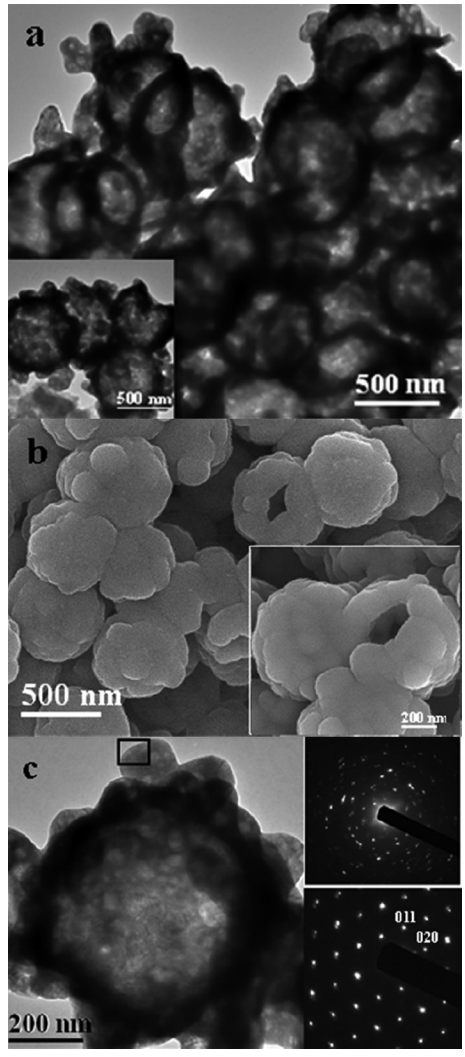

Figure 2. Panoramic (a) TEM and (b) SEM images of the as-prepared $BiVO_4$ hollow nanospheres; the bottom insets are the corresponding magnified images; (c) TEM image of one single $BiVO_4$ hollow nanosphere; the top and bottom insets are the SAED patterns of the whole nanosphere and the rectangle-involved nanoparticle, respectively.

inset of Figure 2c) of the whole spherical shell indicates the polycrystalline nature of the shell, which is consistent with the hierarchical structures observed in the SEM images. However, the SAED pattern of a single nanoparticle (rectangle marked) in Figure 2c shows well-aligned diffraction spots, indicating the primary spherical nanoparticles are singly crystalline (bottom inset of Figure 2c).

Growth Mechanism of the $BiVO_4$ Hollow Nanospheres

In general, hollow structures can be prepared in three steps when CCS is employed as the template:[6b,8a] (1) preparing the CCSs templates; (2) coating the CCSs with designed materials or their precursors; (3) removing the CCSs templates by calcination. For step 1, the CCSs can be easily prepared by polymerization of glucose.[7] Steps 2 and 3, however, are usually challenging. Herein, two stages of heat treatments at different temperatures (80 and 100 °C) were designed to ensure an efficient precipitation of amorphous $BiVO_4$ on the surface of the CCSs. The calcination in stage 3 is aimed at removal of the CCSs templates and promoting crystallization of the amorphous $BiVO_4$ as indicated by the above XRD results. To investigate the detailed growth mechanism of the $BiVO_4$ hollow nanospheres, a series of comparison experiments was carried out.

When the experiment was carried out at 80 °C for 12 h, only Bi_2O_3 was obtained after 2 h of calcination at 350 °C (Figure S2), indicating that Bi^{3+} ions were precipitated on the surface of the CCSs, whereas the VO_3^- ions remained in the EG solvent. Considering the fact that nothing was obtained after 2 h of calcination at 350 °C when the mixed solution was merely stirred at room temperature for 24 h, it is reasonable to speculate that the heat treatment at 80 °C facilitates the precipitation of Bi^{3+} ions on the surface of the CCSs. This precipitation should be attributed to the electrostatic attraction between them, as well as the high activity of Bi^{3+} ions at 80 °C. Moreover, it can be inferred that the other heat treatment at 100 °C promotes the reaction between VO_3^- and the anchored Bi^{3+} and thus amorphous $BiVO_4$ precipitates on the surface of the CCSs.

To further examine the anchoring role of the Bi^{3+} ions in the formation of $BiVO_4$ on the surface of the CCSs, the synthesis was carried out without treatment at 80 °C under otherwise identical conditions. The XRD pattern of the product (Figure S3) shows that all the diffraction peaks can be indexed to *m*-$BiVO_4$, as mentioned above. The SEM image of the product is shown in Figure 3a. It is clear that the product is composed of nanoparticles with sizes of about 50–100 nm. These nanoparticles exhibit a disordered aggregation rather than a hollow-structured assembly. This result implies that direct heat treatment at 100 °C does not establish the effective precipitation of $BiVO_4$ on the surface of the CCSs. By contrast, $BiVO_4$ nanoparticles can be effectively precipitated on the surface of CCSs when the heat treatment at 100 °C was carried out after the one at 80 °C. This comparison experiment confirms the anchoring role of the adsorbed Bi^{3+} ions in the subsequent precipitation of $BiVO_4$ on the surface of the CCSs.

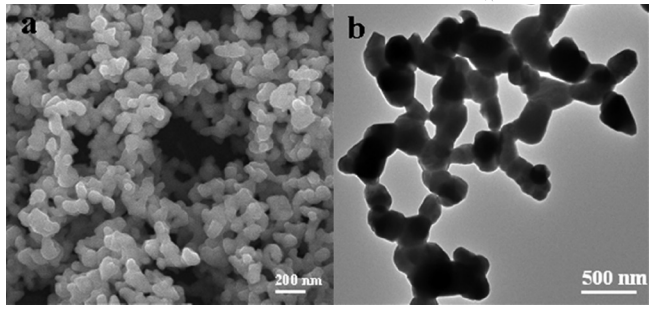

Figure 3. Monoclinic $BiVO_4$ crystals prepared (a) with the oil bath at 80 °C for 12 h and a subsequent calcination at 353 °C for 2 h; (b) with two stages of oil bath at 80 and 100 °C followed by calcination at 450 °C for 2 h.

The appropriate calcination temperature, which is critical for preparation of hollow structures, was determined with DSC and TG analysis on the $BiVO_4$-precipitated CCSs. The results are shown in Figure 4. There are two stages of significant mass loss in the TG process. The first one between 40 and 120 °C corresponds to an endothermic peak in DSC and should be ascribed to the evaporation of adsorbed water. The second one ranging from 331 to 430 °C corresponds to a sharp exothermic peak centered at 353 °C, arising from the oxidation of the CCSs. Besides these two, an exothermic peak centered at 236 °C exists in the DSC curve. Nonetheless, there is no mass change in this stage. To clarify the nature of this process, the $BiVO_4$-precipitated CCSs were calcined at 236 °C for 2 h and the phases of the product were identified with XRD. It is obvious that only diffraction peaks corresponding to *m*-$BiVO_4$ crystals were detected in the XRD pattern (Figure 1b), revealing that the exothermic peak centered at 236 °C should come from the crystallization of amorphous $BiVO_4$ into *m*-$BiVO_4$. On the basis of the analysis above, the peak temperature of 353 °C was determined to remove the CCSs through calcination.

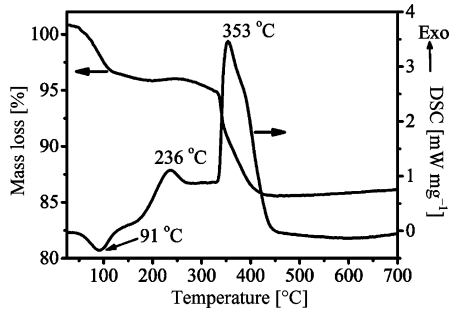

Figure 4. Thermogravimetric (TG) and differential scanning calorimetric (DSC) curves of the $BiVO_4$-precipitated CCSs (heating rate: 5 °C min^{-1}; air atmosphere).

To demonstrate the critical role of the optimum calcination temperature in the preparation of $BiVO_4$ hollow nanospheres, the calcination was also carried out at 450 °C, a temperature previously used in the preparation of hollow-structured simple metal oxides.[8b] The XRD pattern of the product presented in Figure 1d shows pure *m*-$BiVO_4$ crystals. Figure 3b is the TEM image of the corresponding

product. It is obvious that $BiVO_4$ hollow structures have not been obtained. Such a $BiVO_4$ product is composed of circle- and chain-like particles with a size of about 200–250 nm. These particles are larger than those in the $BiVO_4$ hollow nanospheres, which should be due to the growth of $BiVO_4$ nanoparticles at the higher calcination temperature.

On the basis of the above comparison, the growth mechanism of the $BiVO_4$ hollow nanospheres was proposed as follows and illustrated in Scheme 1. When a mixed solution of $Bi(NO_3)_3$ and NH_4VO_3 was heated at 80 °C, Bi^{3+} ions were adsorbed on the negatively charged surface of the CCSs through electrostatic attraction and worked as anchors. Then, with the heating temperature increased to 100 °C, VO_3^- ions in the solution reacted with the anchored Bi^{3+} ions, and amorphous $BiVO_4$ nanoparticles were thus precipitated on the surface of the CCSs to form the $BiVO_4$-precipitated CCSs. Subsequent calcination of $BiVO_4$-precipitated CCSs resulted in the crystallization of amorphous $BiVO_4$ into *m*-$BiVO_4$ at about 236 °C and the removal of the CCS templates at 353 °C. Consequently, the $BiVO_4$ hollow nanospheres were obtained.

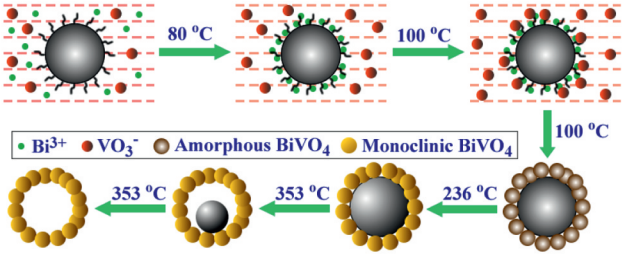

Scheme 1. Schematic growth mechanism of the $BiVO_4$ hollow nanospheres prepared by using colloidal carbon spheres as templates.

Photophysical Properties and Photocatalytic Activity of the $BiVO_4$ Hollow Nanospheres

As was reported, *m*-$BiVO_4$ crystals exhibit high activities not only for photocatalytic degradation of organic contaminants,[11,12] but also for photocatalytic O_2 evolution from aqueous $AgNO_3$ solutions.[13,14] In addition, $BiVO_4$ with tube-like[15] and mesoporous structures[16] exhibit enhanced photocatalytic efficiencies. Therefore, the photophysical properties and photocatalytic activity of the $BiVO_4$ hollow nanospheres were investigated. For comparison, *m*-$BiVO_4$ crystals were also synthesized by a solid-state[17] reaction (SSR-$BiVO_4$) and by an aqueous[18] method (AM-$BiVO_4$). The photocatalytic degradations of RhB and CH_3CHO were carried out over the SSR-$BiVO_4$ and AM-$BiVO_4$ under otherwise identical conditions.

Figure 5 represents the diffuse reflection spectra (DRS) of the $BiVO_4$ hollow nanospheres, AM-$BiVO_4$, and SSR-$BiVO_4$. The former two samples possess an absorption band from 470 to 550 nm, whereas SSR-$BiVO_4$ shows one from 470 to 600 nm. The absorption edges of the $BiVO_4$ hollow nanospheres and the AM-$BiVO_4$ show a steep edge, indicating that visible-light absorption is attributed to the band gap transition rather than the transition from an impurity level.[19] The absorption edge of the SSR-$BiVO_4$, however, shows a prolonged absorption tail besides the steep absorption edge, which should be due to crystal defects arising from the volatilization of reactants at high temperature.[13] According to a reported method,[20] the band gaps (E_g) are calculated to be 2.36, 2.28, and 2.23 eV for the $BiVO_4$ hollow nanospheres, AM-$BiVO_4$, and SSR-$BiVO_4$, respectively (Table S1).

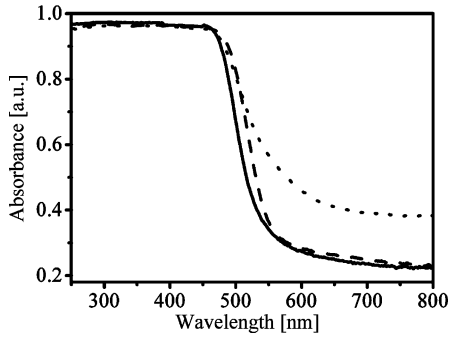

Figure 5. Diffuse reflectance spectra of the $BiVO_4$ hollow nanospheres (solid line), AM-$BiVO_4$ (dashed line), and SSR-$BiVO_4$ (dotted line).

Figure 6 shows the decrease in RhB (C/C_0) as a function of irradiation time over the $BiVO_4$ hollow nanospheres, AM-$BiVO_4$, and SSR-$BiVO_4$. Here, C is the absorption of RhB at a wavelength of 553 nm and C_0 is the absorption of RhB after the adsorption equilibrium between the photocatalyst and the RhB before irradiation. It was confirmed that the photolysis of RhB under visible-light irradiation was negligible.[12] It is clear that the RhB is completely degraded after 70 min of irradiation over the $BiVO_4$ hollow nanospheres (Figure 6a). However, only about 12.5% of RhB can be degraded over the SSR-$BiVO_4$ and 85% over the AM-$BiVO_4$ after 120 min of irradiation (Figure 6b,c). This result demonstrates a much higher photocatalytic efficiency of the $BiVO_4$ hollow nanospheres.

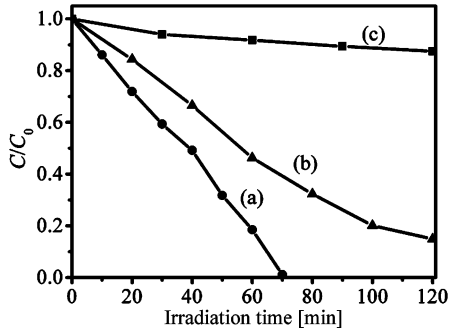

Figure 6. Decrease in RhB (C/C_0) (100 mL, 10^{-4} M) as a function of irradiation time over 0.1 g of the $BiVO_4$ hollow nanospheres (a), AM-$BiVO_4$ (b), and SSR-$BiVO_4$ (c) under visible light ($\lambda >$ 420 nm).

As a typical indoor air contaminant without light absorption and consequent photosensitization during photodegradation process,[21] gaseous CH_3CHO was employed to

confirm the photocatalytic activity of the $BiVO_4$ hollow nanospheres. Figure 7 shows the increase in evolved CO_2 with the irradiation time during the photocatalytic decomposition of CH_3CHO (δ = 100 ppm) over 0.1 g of $BiVO_4$ hollow nanospheres, AM-$BiVO_4$, and SSR-$BiVO_4$ under visible light ($\lambda > 420$ nm). The given amount of CH_3CHO is completely degraded into CO_2 after 6 h of irradiation over the $BiVO_4$ hollow nanospheres (Figure 7a). After the same time of irradiation, however, only 59% (Figure 7b) and 34% (Figure 7c) of CH_3CHO were degraded over the AM-$BiVO_4$ and SSR-$BiVO_4$, respectively. This result further demonstrates the higher photocatalytic efficiency of the $BiVO_4$ hollow nanospheres under visible light. Moreover, the photolysis of CH_3CHO was also carried out under visible light, which reveals the photolysis of ca. 14% of CH_3CHO when irradiated for 6 h and thus confirms the photocatalytic degradation of CH_3CHO.

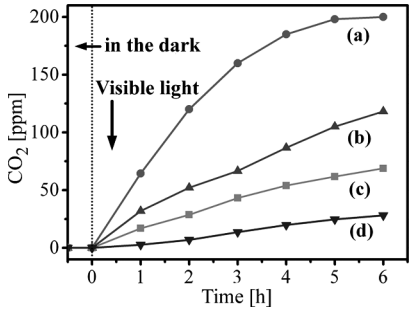

Figure 7. Photocatalytic oxidative decomposition of gaseous acetaldehyde over 0.1 g of $BiVO_4$ hollow nanospheres (a), AM-$BiVO_4$ (b), SSR-$BiVO_4$ (c), and without photocatalyst (d) under visible-light ($\lambda > 420$ nm) irradiation.

As reported,[22] the high BET surface area (S_{BET}) and large band gap played a leading role in improving the photocatalytic activity of the hollow-structured nanospheres. The BET surface area of the $BiVO_4$ hollow nanospheres is 5.85 $m^2 g^{-1}$, which is larger than that of the AM-$BiVO_4$ (3.13 $m^2 g^{-1}$), and SSR-$BiVO_4$ (0.26 $m^2 g^{-1}$) (Table S1). This brings not only more surface reached by visible light and contacted with RhB but also more active catalytic sites.[10] The larger band gap (2.36 eV) of the $BiVO_4$ hollow nanospheres brings about a more powerful redox ability.[23] Thus, the $BiVO_4$ hollow nanospheres exhibited a higher photocatalytic activity than the other two $BiVO_4$ crystals.

Conclusions

m-$BiVO_4$ hollow nanospheres, with diameters of about 700 nm and consisting of 100–150 nm nanoparticles, were successfully synthesized with the use of an anchoring method by employing CCSs as hard templates. In the anchoring synthesis, heat treatment at 80 °C established the effective precipitation of Bi^{3+} ions on the surface of the CCSs to work as anchors. The following heat treatment at 100 °C took a leading role in promoting the reaction between VO_3^- ions and the anchored Bi^{3+} ions, by which amorphous $BiVO_4$ was precipitated on the surface of the CCSs. The subsequent calcinations brought about the crystallization of amorphous $BiVO_4$ into *m*-$BiVO_4$ at about 236 °C and the removal of CCS templates at about 353 °C. The as-prepared $BiVO_4$ hollow nanospheres exhibited a higher photocatalytic activity than AM-$BiVO_4$ and SSR-$BiVO_4$ not only in the degradation of RhB but also in the decomposition of CH_3CHO under visible-light irradiation as a result of their higher BET surface area (5.85 $m^2 g^{-1}$) and larger band gap (2.36 eV). This facile anchoring method provides a possible route to other hollow-structured multicomponent oxides as the general adsorption of metal ions on the negatively charged CCSs.

Experimental Section

Preparation of CCSs: All the reagents were of analytical purity, purchased from Shanghai Chemical Reagent Company, and used without further purification. CCSs were prepared by the polymerization of glucose according to a literature procedure.[7] Glucose (4 g) was dissolved in deionized water (40 mL) to form a clear solution. The solution was added into a 50-mL Teflon-sealed autoclave and kept at 160 °C for 6 h. After the autoclave was cooled down naturally to room temperature, the resulting precipitates were collected, washed with deionized water and absolute ethanol, and dried at 60 °C for 6 h.

Synthesis of $BiVO_4$ Hollow Nanospheres: In a typical synthesis of $BiVO_4$ hollow nanospheres, $Bi(NO_3)_3 \cdot H_2O$ (1.5 mmol) was dissolved in ethylene glycol (20 mL). Black CCSs (0.05 g) was then added into the EG solution and dispersed under magnetic stirring at room temperature. Subsequently, a NH_4VO_3 solution (15 mL, 0.1 M), which was prepared by dissolving NH_4VO_3 into EG at 60 °C, was added to the $Bi(NO_3)_3$ solution whilst stirring. The mixed solution was heated at 80 °C for 12 h and then at 100 °C for 12 h. Then, after three cycles of washing and centrifugation, the brown sample was dried at 60 °C for 6 h. Afterwards, the dried sample was calcined at 353 °C for 2 h in air.

Characterization: The X-ray diffraction (XRD) patterns of the samples were measured with a Rigaku D/Max-2200PC diffractometer using monochromated Cu-K_α radiation (λ = 0.15418 nm) at a scanning rate of 8°/min. The morphologies and microstructures were examined using a field emission scanning electron microscope (FE-SEM, JEOL JSM-6700F) and a transmission electron microscope (TEM, JEOL JEM-2100F) at an accelerating voltage of 200 kV. The diffuse reflectance spectra (DRS) of the $BiVO_4$ samples and the UV/Vis absorption spectra of the RhB solutions were obtained with a Hitachi U-3010 UV/Vis spectrophotometer. Differential scanning calorimetry (DSC) and thermogravimetry (TG) were carried out with a Netzsch STA-409PC/4/H Luxx simultaneous TG-DTA/DSC apparatus with a heating rate of 5 °C min^{-1} from room temperature to 700 °C in air. The Brunauer–Emmett–Teller (BET) surface areas were estimated by N_2 adsorption data with the use of a Micromeritics ASAP2010 Analyzer.

Photocatalytic Activities: The photocatalytic activity of the $BiVO_4$ hollow nanospheres was evaluated by the degradation of RhB and CH_3CHO under visible-light irradiation. The visible light ($\lambda >$ 420 nm) was provided by a 500 W Xe lamp (Shanghai Yaming Lighting Co. Ltd.) with a 420 nm cutoff filter. For degradation of RhB, the photocatalyst (0.1 g) was added to an RhB solution (100 mL, 10^{-5} M). The suspension was then stirred in the dark for 12 h to ensure an adsorption/desorption equilibrium between RhB

and the photocatalyst. After that, the suspension was exposed to visible light under magnetic stirring. At given time intervals, an aliquot (3 mL) of the suspension was sampled and centrifuged to remove the photocatalyst particles. The concentrations of the RhB solutions were monitored with a Hitachi U-3010 UV/Vis spectrophotometer. For degradation of CH_3CHO, the photocatalyst powder (0.1 g) was uniformly spread on a glass plate (ϕ = 15 mm) and placed at the bottom of a gas-closed cylindrical glass vessel with a capacity of ca. 600 mL. Then, gaseous CH_3CHO (δ = 100 ppm, ca. 20 mL) was injected into the vessel, which was filled with ambient air. After the adsorption of CH_3CHO reached equilibrium in the dark in 30 min, irradiation with visible light was performed through a top quartz window of the glass vessel. At 1 h intervals, an aliquot (1.5 mL) of the gas sample was extracted and the amount of carbon dioxide in it was measured by a gas chromatograph (GC 7890II, Shanghai Techcomp Scientific Instruments Co. Ltd.) equipped with a flame ionization detector (N_2 carrier) and a catalytic conversion furnace.

Supporting Information (see footnote on the first page of this article): TEM image of the CCSs; XRD patterns of the product prepared with 12 h of heat treatment at 80 °C and 2 h of calcination at 353 °C and with 12 h of heat treatment at 100 °C and 2 h of calcination at 353 °C; band gaps (E_g) and BET surface areas (S_{BET}) of the $BiVO_4$ hollow nanospheres, AM-$BiVO_4$, and SSR-$BiVO_4$.

Acknowledgments

We acknowledge financial support from the National Natural Science Foundation of China (No. 50672117, 50732004), National Basic Research Program of China (973 Program, 2007CB613305), and the Nanotechnology Programs of Science and Technology Commission of Shanghai (0852nm00500).

[1] a) X. W. Lou, L. A. Archer, *Adv. Mater.* **2008**, *20*, 1853–1858; b) C. Z. Wu, Y. Xie, L. Y. Lei, S. Q. Hu, C. Z. OuYang, *Adv. Mater.* **2006**, *18*, 1727–1732; c) S. Zeng, K. Tang, T. Li, Z. Liang, D. Wang, Y. Wang, W. Zhou, *J. Phys. Chem. C* **2007**, *111*, 10217–10225.

[2] a) P. A. Wingert, H. Mizukami, A. E. Ostafin, *Nanotechnology* **2007**, *18*, 295707; b) Q. Zhao, Y. Gao, X. Bai, C. Wu, Y. Xie, *Eur. J. Inorg. Chem.* **2006**, 1643–1648; c) J. Gao, Q. Li, H. Zhao, L. Li, C. Liu, Q. Gong, L. Qi, *Chem. Mater.* **2008**, *20*, 6263–6269.

[3] a) H. Yu, J. Yu, B. Cheng, S. Liu, *Nanotechnology* **2007**, *18*, 065604; b) H. Li, Z. Bian, J. Zhu, D. Zhang, G. Li, Y. Huo, H. Li, Y. Lu, *J. Am. Chem. Soc.* **2007**, *129*, 8406–8407.

[4] a) Y. Zhu, J. Shi, W. Shen, X. Dong, J. Feng, M. Ruan, Y. Li, *Angew. Chem. Int. Ed.* **2005**, *44*, 5083–5087; b) Y. Cai, H. Pan, X. Xu, Q. Hu, L. Li, R. Tang, *Chem. Mater.* **2007**, *19*, 3081–3083; c) M. Y. Ma, Y. J. Zhu, L. Li, S. W. Cao, *J. Mater. Chem.* **2008**, *18*, 2722–2727.

[5] J. Chen, F. Saeki, B. J. Wiley, H. Cang, M. J. Cobb, Z. Y. Li, L. Au, H. Zhang, M. B. Kimmey, X. Li, Y. Xia, *Nano Lett.* **2005**, *5*, 473–477.

[6] a) F. Caruso, R. A. Caruso, H. Mohwald, *Science* **1998**, *282*, 1111–1114; b) X. W. Lou, L. A. Archer, Z. Yang, *Adv. Mater.* **2008**, *20*, 3987–4019.

[7] X. M. Sun, Y. D. Li, *Angew. Chem. Int. Ed.* **2004**, *43*, 597–601.

[8] a) X. M. Sun, Y. D. Li, *Angew. Chem. Int. Ed.* **2004**, *43*, 3827–3831; b) X. M. Sun, J. F. Liu, Y. D. Li, *Chem. Eur. J.* **2006**, *12*, 2039–2047; c) H. S. Qian, G. F. Lin, Y. X. Zhang, P. Gunawan, R. Xu, *Nanotechnology* **2007**, *18*, 355602; d) X. Wang, P. Hu, F. L. Yuan, L. J. Yu, *J. Phys. Chem. C* **2007**, *111*, 6706–6712; e) Z. Guo, J. Y. Liu, Y. Jia, X. Chen, F. L. Meng, M. Q. Li, J. H. Liu, *Nanotechnology* **2008**, *19*, 345704.

[9] S. H. Li, E. B. Wang, C. G. Tian, B. D. Mao, Z. H. Kang, Q. Y. Li, G. Y. Sun, *J. Solid State Chem.* **2008**, *181*, 1650–1658.

[10] M. Shang, W. Wang, H. Xu, *Cryst. Growth Des.* **2009**, *9*, 991–996.

[11] a) L. Zhou, W. Z. Wang, S. W. Liu, L. S. Zhang, H. L. Xu, W. Zhu, *J. Mol. Catal. A* **2006**, *252*, 120–124; b) M. Long, W. M. Cai, J. Cai, B. X. Zhou, X. Y. Chai, Y. H. Wu, *J. Phys. Chem. B* **2006**, *110*, 20211–20216; c) X. Zhang, Z. Ai, F. Jia, L. Zhang, X. Fan, Z. Zou, *Mater. Chem. Phys.* **2007**, *103*, 162–167.

[12] Y. Zhao, Y. Xie, X. Zhu, S. Yan, S. X. Wang, *Chem. Eur. J.* **2008**, *14*, 1601–1606.

[13] A. Kudo, K. Omori, H. Kato, *J. Am. Chem. Soc.* **1999**, *121*, 11459–11467.

[14] a) S. Tokunaga, H. Kato, A. Kudo, *Chem. Mater.* **2001**, *13*, 4624–4628; b) J. Q. Yu, A. Kudo, *Adv. Funct. Mater.* **2006**, *16*, 2163–2169; c) D. N. Ke, T. Y. Peng, L. Ma, P. Cai, P. Jiang, *Appl. Catal. A: Gen.* **2008**, *350*, 111–117.

[15] a) L. Zhou, W. Wang, L. Zhang, H. Xu, W. Zhu, *J. Phys. Chem. C* **2007**, *111*, 13659–13664; b) L. Ren, L. Jin, J. B. Wang, F. Yang, M. Q. Qiu, Y. Yu, *Nanotechnology* **2009**, *20*, 115603.

[16] T. Li, Z. Zhuo, S. Zhao, Y. G. Wang, *Laser Phys. Lett.* **2008**, *5*, 350–352.

[17] M. Gotić, S. Musić, M. Ivanda, M. Šoufek, S. Popović, *J. Mol. Struct.* **2005**, *744*, 535–540.

[18] S. Kohtani, S. Makino, A. Kudo, K. Tokumura, Y. Ishigaki, T. Matsunaga, O. Nikaido, K. Hayakawa, R. Nakagaki, *Chem. Lett.* **2002**, *31*, 660–661.

[19] A. Kudo, I. Tsuji, H. Kato, *Chem. Commun.* **2002**, 1958–1959.

[20] a) L. Zhou, W. Z. Wang, S. W. Liu, L. S. Zhang, H. L. Xu, W. Zhu, *J. Mol. Catal. A* **2006**, *252*, 120–124; b) M. A. Butler, *J. Appl. Phys.* **1977**, *48*, 1914.

[21] S. Sun, W. Wang, L. Zhang, L. Zhou, W. Yin, M. Shang, *Environ. Sci. Technol.* **2009**, *43*, 2005.

[22] a) J. Yu, X. Yu, B. Huang, X. Zhang, Y. Dai, *Cryst. Growth Des.* **2009**, *9*, 1474–1480; b) B. Li, Y. Xie, M. Jing, G. Rong, Y. Tang, G. Zhang, *Langmuir* **2006**, *22*, 9380–9385.

[23] J. C. Yu, L. Z. Zhang, J. G. Yu, *Chem. Mater.* **2002**, *14*, 4647–4653.

Received: July 1, 2009
Published Online: September 10, 2009

